



means to prepare an ordered nanoporous structure with low cost and nontoxic nonsurfactant templating route *via* sol-gel process.<sup>14-21</sup> Diblock copolymers are especially expected to show a number of advantages for directing ordered growth which include chemical compatibility of the polymeric amphiphiles with the desired material, ease of chemical modification to the amphiphile, the ability to vary pore size and wall thickness by changing the molecular weight of the block copolymer, and, the dimensions of the hydrophilic and hydrophobic blocks comprising the polymer. The building blocks of these diblock copolymers were comprised of the hydrophilic groups of monomethoxy poly(ethylene glycol) (MPEG) and the hydrophobic groups of poly(D,L-lactide) (PDLLA). Templating copolymers were prepared using a ring-opening copolymerization synthesis procedure as shown in Scheme 1.

In this article, we report on how the physical property of synthesized diblock copolymer can affect the formation of ordered nanoporous composite with a suggested mechanism including a thermal stability and morphology.

### Experimental Section

**Materials.** All of chemicals—monomethoxy poly(ethylene glycol) (MPEG,  $M_n=5000, 2000$ ), D,L-lactide (DLLA), stannous 2-ethylhexanoate, tetraethylorthosilicate (TEOS), diethyl ether, methylene chloride, tetrahydrofuran, and toluene were obtained from Aldrich.

**Polymer Preparation.** The polymerization of MPEG-*b*-PDLLA diblock copolymer was performed in dry toluene. Monomethoxy poly(ethyleneglycol) (MPEG) (8 g, 1.60 mmole) was added to 70 mL of dried toluene. The residual water was removed by azeotropic distillation to a final volume of 30 mL. D,L-lactide (DLLA) (1 to 4.4 g, 6.95 to 30.56 mmole) and stannous 2-ethylhexanoate (1 to 8.7 mg, 2.47 to 21.47 mmole) were added to the MPEG/toluene solution and refluxed under a nitrogen atmosphere for 24 h. The solution was precipitated by ether, and methylene chloride. The residual solvent was eliminated by vacuum and the white powder product obtained. The critical micelle concentration (CMC) was determined by a dye solubilization method using a UV-Vis spectrometer. To a series of 5 mL solutions with various block copolymer concentrations, 50  $\mu$ L of 1,6-diphenyl-1,3,5-hexatriene (DPH) solution (0.4 mM in methanol) was added and equilibrated for 30 min. The absorption spectra of these solutions were recorded from 200 to 800 nm. Absorbance at 356 nm was plotted against concentration and the crossing point of the extrapolated two straight lines was defined as CMC.

**Instrumentation.** Molecular weight and molecular weight distribution were obtained by Waters gel permeation chromatography (GPC) relative to a polystyrene standard. The polymer was loaded in THF solution with 1.0 mL/min of flow rate. The nitrogen adsorption and desorption isotherms were measured using a Quantachrome Autosorb-6 system. The sample was pretreated at 100 °C overnight in the vacuum line. The pore size distributions were calculated

from the analysis of the adsorption branch of the isotherm using the Barrett-Joyner-Halenda (BJH) method. The pore volume was taken at the five points of  $P/P_0$ . The 75 MHz  $^{13}\text{C}$  and 59 MHz  $^{29}\text{Si}$  solid-state NMR experiments were carried out using a Chemagnetics spectrometer (300 MHz, 89 mm wide bore Oxford magnet). The samples were loaded into 7 mm Zirconia PENCIL rotors and spun at 3-4 kHz. For all experiments, 40-ms acquisition times and a 50 kHz spectral window were employed. The number of transients was 500-5000. Both single-pulse (SP) Bloch-decay and cross polarization (CP) methods were used with and without 1H decoupling. SP spectra were collected using a 4.5  $\mu$ s ( $90^\circ$ )  $^{13}\text{C}$  pulse and a 30s repetition delay. The power levels of the carbon and proton channels were set so that the Hartmann-Hahn match was achieved at 32.5 kHz in CP experiments. The Lorentzian line broadening of 24 Hz was used for all  $^{13}\text{C}$  (SP) spectra, while 50 Hz was used for  $^{29}\text{Si}$  NMR spectrum. The liquid-state  $^{13}\text{C}$  and  $^1\text{H}$  NMR spectra for the block copolymer solutions were collected on a Varian VXR-300 spectrometer using a Doty Scientific, Inc. probe. Chemical shifts were referenced to DMSO at 39.5 ppm.

### Results and Discussion

**Characterization of Diblock Copolymers.** The ring-opening polymerization was used to the synthesis of MPEG-*b*-PDLLA block copolymers that were used as an organic template. The yield is up to 85% with the fractional precipitation method. Modifying the chain length of the resident hydrophilic and hydrophobic groups in the polymer could systematically control the pore diameter and wall

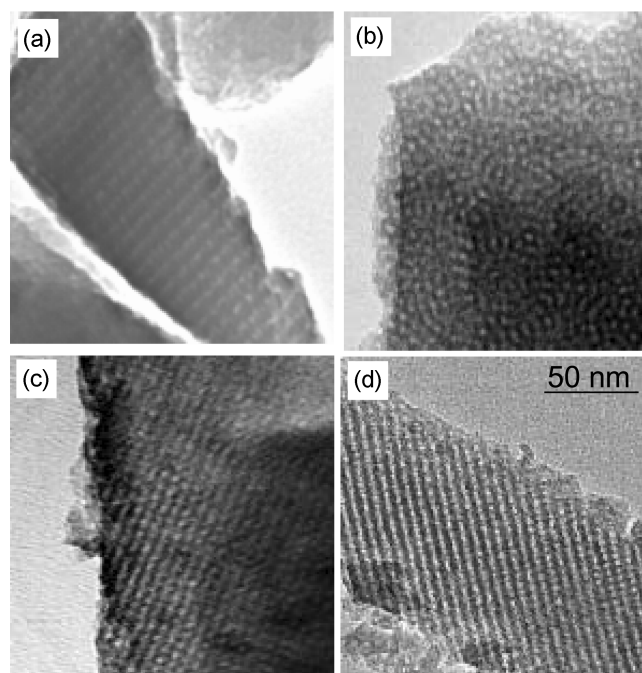


**Figure 1.** TEM images of nanoporous silica derived from the block copolymer templates. The  $M_n$  values of MPEG-*b*-PDLLA are as follows: (a) 5000-600, (b) 5000-1150, (c) 2000-163, and (d) 2000-500.

thickness of the self-assembled nanostructure. Polydispersity values of the synthesized block copolymers were determined from GPC measurements with a Waters refractive index detector and a Wyatt Technology mini DAWN multiangle light scattering detector and <sup>1</sup>H-NMR spectra also were measured by relative integration ratio of the peak areas. <sup>1</sup>H-NMR shows four peaks as assigned as followed: δ 1.6 (d, CH<sub>3</sub> for PDLLA), δ 3.4 (s, OCH<sub>3</sub> for MPEG), δ 3.6 (m, CH<sub>2</sub>CH<sub>2</sub>O for PEG), δ 4.4 (m, COOCH<sub>2</sub> for the oxymethylene bound to the PDLLA). In addition, the critical micelle concentration (CMC) of each block copolymer was determined by means of a dye-solubilization method. The CMC could be decreased to lower concentrations from 1 to about 0.01 wt% with an increase in chain length of the block copolymer.

**Nanoporous Silica from Controlled Micelle Size.** Ordered nanoporous ceramic oxides were prepared from the block

copolymer : 0.8 M-HCl : H<sub>2</sub>O : TEOS in the following wt% ratios, 1 : 24 : 4 : 5, respectively. The micelle concentration of this solution is higher than the CMC. After calcinations at 550 °C for 6 hours, the nanoporous silica obtained from block copolymer templates with various hydrophilic and hydrophobic chain lengths shows a specific surface area of up to 657 m<sup>2</sup>/g, as determined from nitrogen BET measurements. Figure 1 shows the TEM images of these materials, which exhibit a hexagonal array of lattice fringes as well as parallel fringes corresponding to the side-on view of the pores. The pore size increases from 2 nm through 8 nm with the increase of hydrophobic chain length. The worm-like pore structures are obtained from the longer hydrophilic and hydrophobic chain length due to the size of micelle structures. Based on the hydrophilic domain, the shorter domain in block copolymer gives a sophisticated pre-structures rather than the larger domain. Both nitrogen

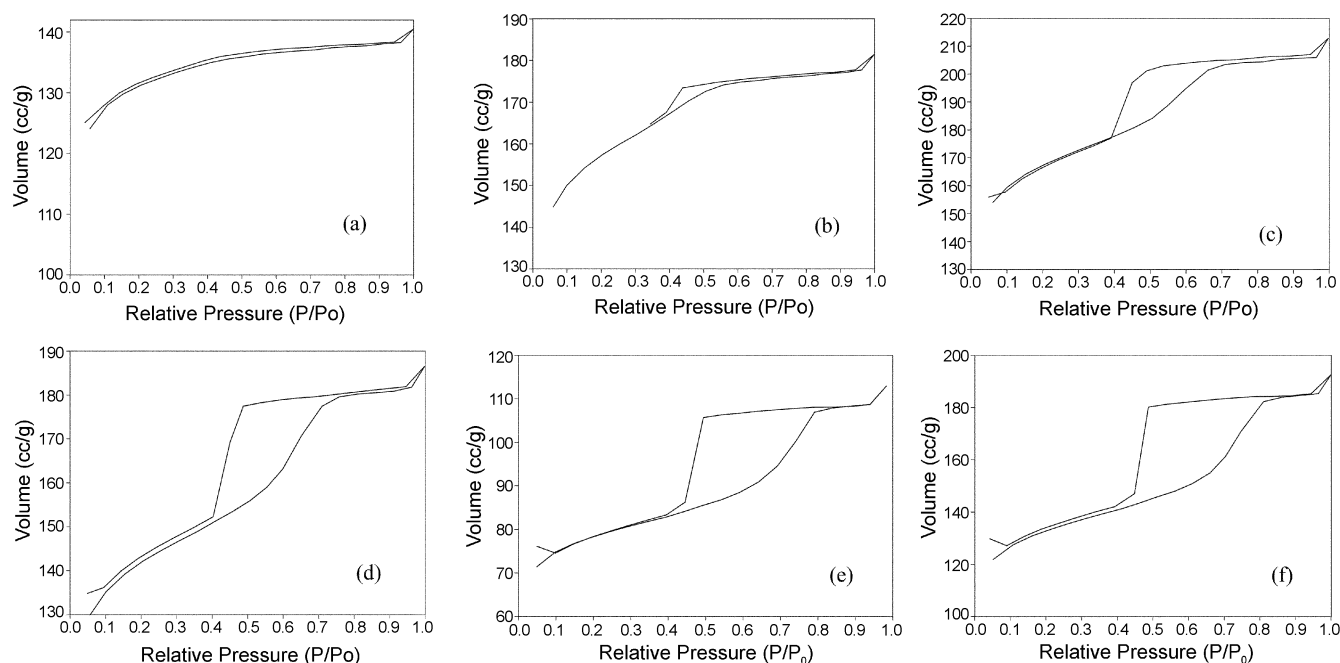


**Figure 2.** Nitrogen adsorption-desorption isotherm plots of nanoporous silica from MPEG-*b*-PDLLA: (A) 5000-320, (B) 5000-600, (C) 5000-1150, (D) 5000-1300, (E) 5000-1560, and (F) 5000-1750.

**Table 1.** The physical parameters of nanoporous silica from MPEG-*b*-PDLLA

| Sample name | MPEG- <i>b</i> -PDLLA |                 |                 | Surface Area (m <sup>2</sup> /g) | Pore size (Å) | Wall thickness (Å) | Pore volume (cm <sup>3</sup> /g) |
|-------------|-----------------------|-----------------|-----------------|----------------------------------|---------------|--------------------|----------------------------------|
|             | P.D <sup>a</sup>      | Mn <sup>a</sup> | Mn <sup>b</sup> |                                  |               |                    |                                  |
| A           | 1.11                  | 5000-340        | 5000-320        | 391                              | —             | —                  | 0.14                             |
| B           | 1.15                  | 5000-620        | 5000-600        | 496                              | 38            | 48                 | 0.76                             |
| C           | 1.21                  | 5000-1270       | 5000-1150       | 657                              | 55            | 52                 | 0.79                             |
| D           | 1.24                  | 5000-1450       | 5000-1300       | 638                              | 61            | 54                 | 0.68                             |
| E           | 1.22                  | 5000-1680       | 5000-1560       | 652                              | 74            | 65                 | 0.47                             |
| F           | 1.29                  | 5000-1900       | 5000-1750       | 634                              | 80            | 70                 | 0.41                             |
| G           | 1.25                  | 2000-50         | 2000-40         | 370                              | —             | —                  | 0.11                             |
| H           | 1.18                  | 2000-80         | 2000-62         | 385                              | —             | —                  | 0.17                             |
| I           | 1.14                  | 2000-150        | 2000-163        | 427                              | 26            | 32                 | 0.39                             |
| J           | 1.16                  | 2000-550        | 2000-500        | 467                              | 34            | 43                 | 0.57                             |

<sup>a</sup>Determined by GPC. <sup>b</sup>Determined by <sup>1</sup>H-NMR. (P.D: polydispersity, Mn: unit molecular weight)

adsorption-desorption isotherms are represented in Figure 2. The adsorption-desorption isotherms show a deviated *type IV* isotherm pattern as the pore size increases confirming a homogeneous distribution of uniform mesoporous structure. This deviation can be explained in terms of a bottleneck shape of the pores, which gives rise to the *type IV* isotherm with a typical *H<sub>2</sub>-type* hysteresis loops, which has a strong steep desorption branch and a more or less sloping adsorption branch. Pore parameters obtained by BET and TEM show that the pore size and wall thickness increase with the chain length of hydrophobic and hydrophilic groups, respectively (Table 1). The relationship between block size ratios in block copolymers and pore size, wall thickness, and micelle size were plotted in Figure 3. Until now, there is few of report on the preparation of the ordered nanoporous materials through the micelle structure mentioned the exact relationship between micelle and formed pore-wall structures. The micelle size was determined by TEM micrographs with 2% uranyl acetate. A copper grid coated with Formvar (polyvinyl formal resin, Monsanto Chem. Co.) and carbon and evaporated micellar suspension were floated face down on the drop for 1 minute. The excess micellar solution was blotted by filter paper. The order of micelle size was found to increase with increasing hydrophobic chain length as shown in Figure 4. This is attributed to the increased core

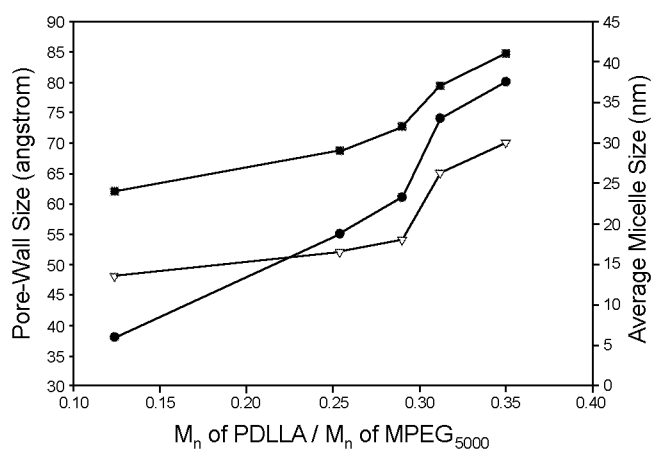


**Figure 3.** Relationships between pore size, wall thickness, and micelle size vs.  $M_n$  fractions of MPEG<sub>5000</sub>-*b*-PDLLA (●; pore size, ▽; wall thickness, and ■; micelle size).

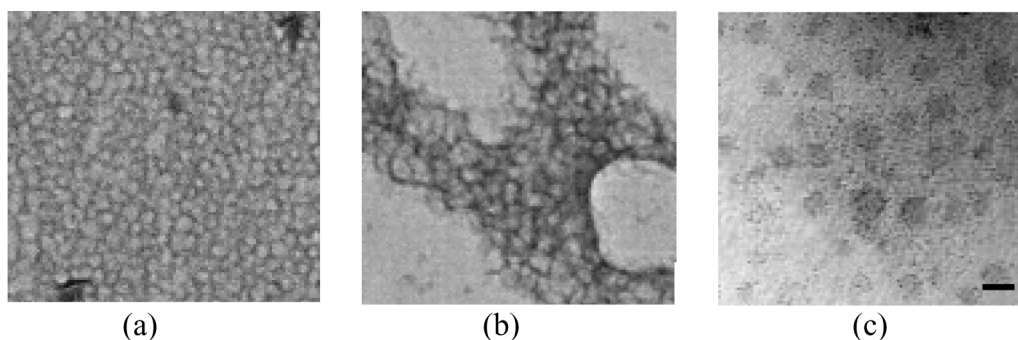
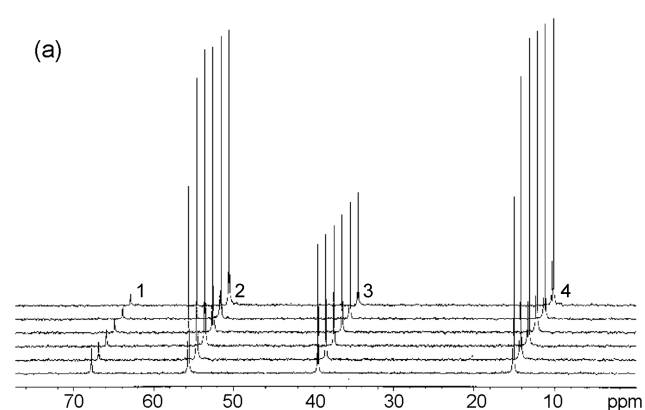


**Figure 4.** Transmission electron micrographs of MPEG-*b*-PDLLA micelles. (a) 5000-620, (b) 5000-1680, (c) 2000-150, and (d) 2000-550 (scale bar: 100 nm)



| Time (min) | Integration values |            |            |            |
|------------|--------------------|------------|------------|------------|
|            | 1 (68 ppm)         | 2 (57 ppm) | 3 (40 ppm) | 4 (16 ppm) |
| 191        | 20                 | 245        | 100        | 270        |
| 164        | 20                 | 242        | 100        | 267        |
| 134        | 19                 | 229        | 100        | 253        |
| 73         | 20                 | 230        | 100        | 254        |
| 45         | 20                 | 220        | 100        | 245        |
| 19         | 28                 | 137        | 100        | 153        |

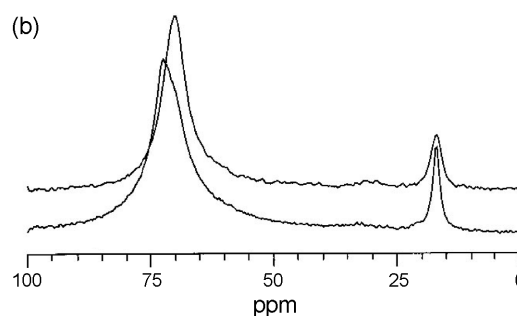


**Figure 5.** Liquid and solid-state  $^{13}\text{C}$  MAS NMR spectra using the MPEG<sub>5000</sub>-*b*-PDLLA<sub>600</sub> template. (a) Time-dependent liquid-state single pulse (SP) spectra with DMSO as an internal standard for 3h after addition of TEOS. The peaks at 68, 56, 40, and 15 ppm correspond to CH<sub>2</sub>O in MPEG, -CH<sub>2</sub> in EtOH, -CH<sub>3</sub> in DMSO and -CH<sub>3</sub> in EtOH, respectively. (b) Solid-state cross polarization (CP) MAS spectra of the pure block copolymer (bottom) and block copolymer-silicate (top).

size resulting from hydrophobic aggregation that involves a higher aggregation number as seen in a previous report.<sup>22</sup> Based upon this finding preparation of any desired pore structure within the tunable range can be achieved.

**The Core-Shell Formation Approach.** Both liquid and solid-state  $^{13}\text{C}$  NMR techniques were used to probe the molecular formation mechanism. Recent papers that described the use of ionic or non-ionic commercially available surfactants as organic templates reported that silica precursors derived from TEOS/TMOS reacted with the micelle surface and formed the silicate wall structure.<sup>23</sup> However, it is very difficult to determine how the surfactant interacts with the silica precursors because such surfactants form a complex charged structure in aqueous solution. In contrast, the use of diblock copolymers allows determination of how and where silica sources bind to the non-ionic surfactants. This is because of the amphiphilic nature of the polymer where the hydrophobic blocks form the core and the hydrophilic blocks form the shell. Time-dependent liquid  $^{13}\text{C}$  NMR spectra along with solid-state MAS NMR spectra were obtained and several features are noteworthy as shown in Figure 5. Figure 5(a) shows a time-dependent  $^{13}\text{C}$  NMR spectra to probe the reaction pathway between copolymer and TEOS. When TEOS was first added to the aqueous polymer solution, the two liquid phases were immiscible and TEOS became gradually hydrolyzed at the interface between the two phases. Due to strong interactions between the partially hydrolyzed TEOS ( $-\text{O}(\text{Si}(\text{OH})(\text{OEt})_2)$ ) and the MPEG of the block copolymer, signals from the partially hydrolyzed TEOS are not observed. The partially hydrolyzed TEOS engages in hydrogen bonding with oxygen in the hydrophilic group of the block copolymer, forming a new hybrid material comprised of block copolymer and silica. This process of converting liquid phase to a gel and solid phase is initially rapid as manifested by a decrease of the MPEG resonance at 68 ppm, the feature associated with EtOH also increases dramatically in the first 45 min. However, it takes 3 hours to form the final solid phase. Thus it is clear from measured liquid-state NMR spectra that the silica, resulting from hydrolyzed TEOS, binds to the hydrophilic region thereby forming the shell structure of the polymer. The integration values are inserted with the reaction time scale. In addition, Figure 5(b) shows the solid-state  $^{13}\text{C}$  NMR spectra of the acquirement of both pure polymer and the final solid precipitate (block copolymer/silicate) to validate the core-shell formation mechanism. Solid-state NMR spectra show two peaks associated with a hydrophilic region (MPEG) and a hydrophobic region (PDLLA) at 70 ppm and 17 ppm, respectively. The feature attributed to the hydrophilic region in the block copolymer-silicate shows a  $\sim 2$  ppm upfield shift as compared with the peak in the pure solid block copolymer. This likely results from the interaction of MPEG with hydrolyzed TEOS. The hydrophobic peak at 17 ppm for the block copolymer/silicate material is broader than that of the pure block copolymer itself. This may be attributed to pore confinement effects in which the hydrophobic region appears to show

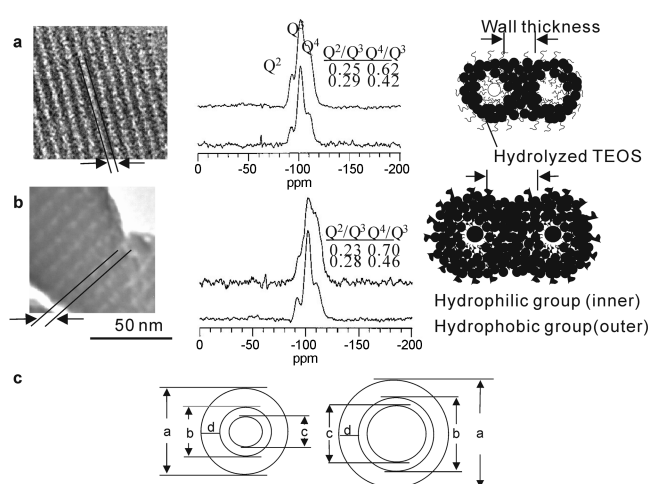


**Figure 6.** Contrasting wall thickness of two nanoporous silicas derived from (a) MPEG<sub>2000</sub>-*b*-PDLLA<sub>500</sub> and (b) MPEG<sub>5000</sub>-*b*-PDLLA<sub>600</sub> templates. TEM images, the CP  $^{29}\text{Si}$  MAS NMR spectra, and quantitative determination of wall thickness are shown. (c) The schematic diagram of core-shell approach. (a, a': micelle diameter, b, b': hydrophobic core, c, c': pore diameter, and d, d': hydrophilic shell)

reduced mobility as confirmed by relaxation time measurements. Both solid and liquid state NMR measurements provide critical data that supports the core-shell formation mechanism.

A comparison of samples B and J, which have similar hydrophobic chain lengths, but different hydrophilic chain lengths, shows an increased wall thickness for materials derived from the longer chain length precursors that comprise the hydrophilic shell even though both resulting materials have a similar pore size. TEM images reveal variations in wall thickness of the calcined silica materials for samples having similar hydrophobic regions in Figure 6(a) and (b). The solid-state  $^{29}\text{Si}$  MAS NMR spectra provide chemical information about the localized silicon environment. Here, three resonances are seen at -91, -102 and -112 ppm, corresponding to  $(\text{HO})_2\text{Si}(\text{OSi})_2$  (Q<sup>2</sup>),  $\text{HOSi}(\text{OSi})_3$  (Q<sup>3</sup>) and  $\text{Si}(\text{OSi})_4$  (Q<sup>4</sup>) silicate species before and after calcination. The ratio of the relative peak areas of Q<sup>4</sup>/Q<sup>3</sup> in the calcined materials of B and J are 0.70 and 0.62, respectively. An increase of the Q<sup>4</sup> resonance intensity is associated with the increased wall thickness since more  $-(\text{OSi})_4$  segments are formed.

The core-shell approaching diagram to formation of pore and wall thickness was suggested and showed some physical property depend on the micelle size in Figure 6(c). The inorganic silicon source (TEOS) occupied the region of (a-c) and (a'-c'). As going to the hydrolysis, the encapsulated TEOS in micelle core by hydrophobic partition is coming out the hydrophilic shell region, (a-c) and (a'-c'). Quantitative determination of wall thickness has been demonstrated with the block copolymer-silica hybrid phase. In contrast, the nanoporous silica derived from a template of the larger hydrophilic shells and hydrophobic cores, has a stable structure consisting of thickened walls and large pore sizes.

### Conclusion

The core-shell approach allows for the preparation of ordered nanoporous ceramic materials that involves a self-assembly process at the molecular level based upon the monomethoxy poly(ethyleneglycol)-*block*-poly(*D,L*-lactide), MPEG-*b*-PDLLA, block copolymer templates. This approach provides for rapid self-assembly and structural reorganization at room temperature. The formation mechanism of these nanoporous structures obtained by controlling the micelle size has been confirmed using both liquid and solid state  $^{13}\text{C}$  and  $^{29}\text{Si}$  NMR techniques. Resulting pore size and wall thickness are closely related to the size of hydrophobic cores and hydrophilic shells of the template. The silica precursor is bound to hydrophilic regions after hydrolysis at the interface of the aqueous phase. Nanostructures obtained are very stable for the thickened wall structures. Results suggest a new core-shell mechanism for nanostructure formation and allow fine-tuning of the pore size and wall thickness using various types of block copolymers as templating agents.

### References and Notes

1. Kresge, C. T.; Leonowicz, M. E.; Roth, W. J.; Vartuli, J. C.; Beck, J. S. *Nature* **1992**, 359, 710.
  2. Yang, H.; Coombs, N.; Ozin, G. A. *Nature* **1997**, 386, 692.
  3. Zhao, D.; Feng, J.; Huo, Q.; Melosh, N.; Fredrickson, G. H.; Chmelka, B. F.; Stucky, G. D. *Science* **1998**, 279, 548.
  4. Kim, S. S.; Zhang, W.; Pinnavia, T. J. *Science* **1998**, 282, 1302.
  5. Braun, P.; Osenar, V. P.; Stupp, S. I. *Nature* **1996**, 380, 325.
  6. Liu, J.; Shin, Y.; Nie, Z.; Chang, J. H.; Wang, L. Q.; Fryxell, G. E.; Samuels, W. D.; Exarhos, G. J. *J. Phys. Chem. A* **2000**, 104, 8328.
  7. Göltner, C. G.; Antonietti, M. *Adv. Mater.* **1997**, 9, 431.
  8. Huo, Q.; Margolese, D. I.; Stucky, G. D. *Chem. Mater.* **1996**, 8, 1147.
  9. Mercier, L.; Pinnavia, T. J. *Chem. Mater.* **2000**, 12, 188.
  10. Zhao, D.; Huo, Q.; Feng, J.; Chmelka, B. F.; Stucky, G. D. *J. Am. Chem. Soc.* **1998**, 120, 6024.
  11. Monnier, A.; Schuth, F.; Huo, Q.; Kumar, D.; Margolese, D.; Maxwell, R. S.; Stucky, G. D.; Krishnamurty, M.; Petroff, P.; Firouzi, A.; Janicke, M.; Chmelka, B. F. *Science* **1993**, 261, 1299.
  12. Steel, A.; Carr, S. W.; Anderson, M. W. *J. Chem. Soc., Chem. Commun.* **1994**, 157.
  13. Chen, C. Y.; Burkett, S. L.; Li, H. X.; Davis, M. E. *Microporous Mater.* **1993**, 2, 27.
  14. Bates, F. S.; Fredrickson, G. H. *Physics Today* **1999**, February, 32.
  15. Jenekhe, S. A.; Chen, X. L. *Science* **1999**, 283, 372.
  16. Chang, J. H.; Jeong, Y. H.; Shin, Y. K. *Bull. Korean Chem. Soc.* **2003**, 24, 119.
  17. Shen, H.; Eisenberg, A. *J. Phys. Chem. B* **1999**, 103, 9473.
  18. Göltner, C.; Henke, G. S.; Weissenberger, M. C.; Antonietti, M. *Angew. Chem. Int. Ed.* **1998**, 37, 613.
  19. Yang, J. H.; Lee, S. Y.; Han, Y. S.; Park, K. C.; Choy, J. H. *Bull. Korean Chem. Soc.* **2003**, 24, 499.
  20. Templin, M.; Franck, A.; Chesne, A. D.; Leist, H.; Zhang, Y.; Ulrich, R.; Schadler, V.; Wiesner, U. *Science* **1997**, 278, 1795.
  21. Finnefrock, A. C.; Ulrich, R. A.; Chesne, D.; Honeker, C. C.; Schumacher, K.; Unger, K. K.; Gruner, S. M.; Wiesner, U. *Angew. Chem. Int. Ed.* **2001**, 40, 1207.
  22. Reley, T.; Stolinik, S.; Heald, C. R.; Xiong, C. D.; Garnett, M. C.; Illum, L.; Davis, S. S.; Purkiss, S. C.; Barlow, R. J.; Gellert, P. R. *Langmuir* **2001**, 17, 3168.
  23. Raman, N. K.; Anderson, M. T.; Brinker, C. J. *Chem. Mater.* **1996**, 8, 1682.
-